Monthly Notices
of the
ROYAL ASTRONOMICAL SOCIETY

MNRAS **485,** 3352–3359 (2019)
Advance Access publication 2019 March 15

doi:10.1093/mnras/stz608

Black hole formation in the context of dissipative dark matter

M. A. Latif,[1]★ A. Lupi,[2] D. R. G. Schleicher,[3]★ G. D'Amico,[4,5] P. Panci[4,6] and S. Bovino[3]

[1]*Physics Department, College of Science, United Arab Emirates University, PO Box 15551 Al-Ain, UAE*
[2]*Scuola Normale Superiore, Piazza dei Cavalieri, 7, I-56126 Pisa, Italy*
[3]*Departamento de Astronomía, Facultad Ciencias Físicas y Matemáticas, Universidad de Concepción, Av. Esteban Iturra s/n Barrio Universitario, Casilla 160-C, Chile*
[4]*CERN Theoretical Physics Department, Case C01600, CH-1211 Geneve, Switzerland*
[5]*Stanford Institute for Theoretical Physics, Stanford University, Stanford, CA 94306, USA*
[6]*Laboratori Nazionali del Gran Sasso, Via G. Acitelli, 22, I-67100 Assergi (AQ), Italy*

Accepted 2019 February 26. Received 2019 February 12; in original form 2018 December 7

ABSTRACT

Black holes with masses of 10^6–$10^9\,M_\odot$ dwell in the centres of most galaxies, but their formation mechanisms are not well known. A subdominant dissipative component of dark matter with similar properties to the ordinary baryons, known as mirror dark matter, may collapse to form massive black holes during the epoch of first galaxies formation. In this study, we explore the possibility of massive black hole formation via this alternative scenario. We perform three-dimensional cosmological simulations for four distinct haloes and compare their thermal, chemical, and dynamical evolution in both the ordinary and the mirror sectors. We find that the collapse of haloes is significantly delayed in the mirror sector due to the lack of H_2 cooling and only haloes with masses above $\geq 10^7\,M_\odot$ are formed. Overall, the mass inflow rates are $\geq 10^{-2}\,M_\odot\,yr^{-1}$ and there is less fragmentation. This suggests that the conditions for the formation of massive objects, including black holes, are more favourable in the mirror sector.

Key words: black hole physics – methods: numerical – galaxies: formation – early Universe – cosmology: theory.

1 INTRODUCTION

Most of the galaxies if not all today harbour supermassive black holes (SMBHs) of a few million to billion solar masses (Kormendy & Ho 2013) and their presence has also been revealed from the observations of quasars up to $z \geq 7$, a few hundred million years after the big bang (Fan et al. 2003; Willott et al. 2007; Jiang et al. 2009; Mortlock et al. 2011; Venemans et al. 2015; Wu et al. 2015; Bañados et al. 2018; Schleicher 2018). The existence of such massive objects at early epochs poses a challenge to our understanding of structure formation in the Universe. How come they formed and how did they grow are still open questions.

Various models of black hole (BH) formation have been proposed in the literature, which include the collapse of stellar remnants, runaway collisions in stellar clusters, and the collapse of a giant gas cloud into a massive BH, i.e. the so-called direct collapse model. These models provide seed BHs of 10–$10^5\,M_\odot$ and these seed BHs have to efficiently grow to reach the observed masses within the first billion years. Population III stars, depending on their mass, may collapse into a BH of a few hundred solar masses. However, they have to continuously grow at the Eddington limit to reach the observed masses. The feedback from BHs halts the accretion on to them (Johnson & Bromm 2007; Alvarez, Wise & Abel 2009; Smith et al. 2018) and they may require a few episodes of super-Eddington accretion (Madau, Haardt & Dotti 2014; Mayer et al. 2015; Inayoshi, Haiman & Ostriker 2016; Lupi et al. 2016) to grow to a billion solar masses. The mass of BHs resulting from runaway collisions in dense stellar clusters depends on the density, metallicity, and the initial mass of the cluster. Under optimal conditions, seed BHs from this scenario can have masses of about a thousand solar masses and have to form within the first 2–3 million years (Portegies Zwart & McMillan 2002; Devecchi et al. 2012; Katz, Sijacki & Haehnelt 2015; Reinoso, Fellhauer & Véjar 2018a; Reinoso et al. 2018b; Sakurai, Yoshida & Fujii 2019). Particularly, the potential interaction between stellar collisions and gas accretion is important. The latter may enhance the BH mass formed in the first stellar clusters (Boekholt et al. 2018), or trigger the formation of run-away mergers in clusters of stellar-mass BHs (Davies, Miller & Bellovary 2011; Lupi et al. 2014). The direct collapse model, on the other hand,

★ E-mail: latifne@gmail.com (MAL); dschleicher@astro-udec.cl (DRGS)

provides BH seeds with masses of about 10^5 $M_\odot$, but requires large inflow rates of about 0.1 $M_\odot$ yr^{-1} (Bromm & Loeb 2003; Schleicher et al. 2013; Latif & Schleicher 2015; Latif, Schleicher & Hartwig 2016c; Becerra et al. 2018; Wise et al. 2019). Such conditions can be achieved in metal free haloes illuminated by strong UV radiation (Chon & Latif 2017). However, it is still not clear what would be the number density of direct collapse BHs. Even very massive seeds would require rather special conditions to efficiently grow, see Latif, Volonteri & Wise (2018) and Regan et al. (2018). Each model has its pros and cons, further details about the models can be found in the dedicated reviews on this topic (Volonteri & Bellovary 2012; Haiman 2013; Latif & Ferrara 2016a; Dayal et al. 2018; Woods et al. 2018).

In this article, we take an alternative approach and explore the possibility of forming massive BHs via dissipative dark matter (DM). D'Amico et al. (2018, hereafter called D18) have proposed that a small component of mirror matter (i.e. an elegant model of dissipative DM; see e.g. Blinnikov & Khlopov 1983; Khlopov et al. 1991; Foot 2004; Berezhiani 2005) may form intermediate-mass BHs. They have shown, using one-zone models, that the thermal and the chemical evolution for both the mirror $\mathcal{M}$ and the ordinary $\mathcal{O}$ sectors are different due to the lower $\mathcal{M}$ radiation temperature. Furthermore, they found that the thermal evolution in the $\mathcal{M}$ sector depends on the virial temperature of the halo and 3D simulations are required to investigate this effect. They also pointed out that, in the presence of this dissipative DM sector, the BHs are expected to grow at a faster rate with respect to the ordinary case as they can accrete both collapsed $\mathcal{O}$ and $\mathcal{M}$ matters. Motivated by the work of D18, we perform two sets of 3D cosmological simulations of the first minihaloes forming at $z = 20$–30, one for the $\mathcal{M}$ sector and other for the $\mathcal{O}$ without the mirror baryons (standard simulations). We explore the impact of hydrodynamics and the collapse dynamics on the thermal and chemical properties of the haloes in the $\mathcal{M}$ sector. We assess the inflow rates, and also study fragmentation properties of these haloes. Our findings suggest that haloes forming in the $\mathcal{M}$ sector are about an order of magnitude more massive and they may have important implications for the formation of first structures in the Universe.

Our article is organized as follows. In Section 2, we describe the model, and the numerical methods and initial conditions. We present our results in Section 3 and confer our conclusions in Section 4.

2 SETTING THE STAGE

2.1 A dissipative DM model

In terms of microphysical properties, a symmetric mirror sector (the parity symmetry which exchanges the $\mathcal{M}$ and $\mathcal{O}$ field is not broken) is identical to the standard model of particle physics, for details see D18 and references therein. The $\mathcal{M}$ sector differs from the $\mathcal{O}$ sector only in two macroscopic quantities: (i) the ratio of abundances $\beta = \Omega_b^{'}/\Omega_b$ and (ii) the ratio of radiation temperatures $x = T_\gamma^{'}/T_\gamma$. The $'$ symbol denotes mirror matter. To avoid stringent BBN and CMB limits, the $\mathcal{M}$ sector must be colder than the ordinary one ($x \lesssim 0.3$; Berezhiani, Comelli & Villante 2001; Berezhiani 2005; Foot & Vagnozzi 2015; Essig et al. 2018). Given the tight constraints on the WIMP paradigm, the debate on the particle physics model of DM is very much open. The mirror model of DM fits in constructions where there are hidden sectors with several fields. These can arise naturally in braneworld constructions in string theory as well.

In our simulations, we assume $\beta = 1$ and $x = 0.01$. The rest of DM is in the form of standard cold and collisionless DM. These values could result from an $\mathcal{M}$ sector with a broken mirror parity (see e.g. Berezhiani, Dolgov & Mohapatra 1996) or a minimal mirror twin Higgs (see e.g. Barbieri, Hall & Harigaya 2016). Although one cannot easily predict typical values for these parameters, we expect that our benchmark model exhibits macrophysical behaviour common to several microphysical realizations of mirror DM. In addition to the β and x parameters, we assume for simplicity that the chemistry is the same in the two sectors. However, one can easily imagine scenarios in which the mirror chemistry makes the production of H_2 more difficult (Rosenberg & Fan 2017). We cannot study these at the moment, but we expect that our benchmark model exhibits similar qualitative features.

For the $\mathcal{M}$ sector, we only consider conventional DM and mirror baryons (i.e. dark baryons) in the simulations and neglect ordinary baryons. These components only interact gravitationally (and via renormalizable portals that we set to zero), so we assume their impact is not strong as on larger scales gravity is dominated by the DM, and on smaller scales self-gravity takes over. To solve the chemical and thermal evolution of $\mathcal{M}$ matter in the early Universe, we follow the approach of D18. They have shown that due to the faster recombination in the $\mathcal{M}$ sector, the fraction of free electrons is lower and results in a suppressed abundance of $\mathcal{M}$ molecular hydrogen.

2.2 Numerical methods

We employ the publicly available code ENZO (Bryan et al. 2014) to conduct hydrodynamical cosmological simulations. ENZO is an open source, adaptive mesh refinement (AMR), parallel, multiphysics simulation code which can run and scale well on various platforms using the message passing interface (MPI). Hydrodynamics is solved using the piecewise parabolic method (PPM) and the DM dynamics is computed with a particle-mesh based *N*-body solver. For self-gravity calculations, we use a multigrid Poisson solver.

We make use of the MUSIC package (Hahn & Abel 2011) to generate cosmological initial conditions typically at $z \geq 100$ by using the PLANCK 2016 data with $\Omega_m = 0.3089$, $\Omega_\Lambda = 0.6911$, $H_0 = 0.6774$ (Planck Collaboration XIII 2016). Our cosmological volume (simulation box) has a comoving size of 1 Mpc h^{-1}, we select the most massive halo forming in our computational domain at $z \geq 20$ and place it at the centre of the box. We employ nested grid initial conditions with a top-level grid resolution of 128^3 cells and an equal number of DM particles. We subsequently employ two additional nested grids each with the same resolution as of the top grid. In addition to this, we further employ 18 additional levels of refinement during the course of the simulations which provide us with an effective resolution of about 200 au. We ensure a Jeans resolution of at least four cells during the simulations. In total, we employ 5767 168 DM particles to solve the *N*-body dynamics which provides us an effective DM resolution of about a few hundred solar masses. Our refinement criterion is based on the baryonic overdensity in both sectors and the DM mass resolution. A cell is marked for refinement when it exceeds four times the cosmic mean density or DM particle density of 0.0625 times $\rho_{DM} r^{\ell\alpha}$ where ρ_{DM} is the DM density, $r = 2$ is the refinement factor, ℓ is the refinement level, and $\alpha = -0.3$ makes the refinement super-Lagrangian.

We use the KROME package (Grassi et al. 2014) to self-consistently solve the thermal and chemical evolution of nine

Table 1. The properties of the simulated haloes are listed here. The second and fourth columns are the halo masses w/o (Halo mass$^{\mathcal{O}}$) and w/ (Halo mass$^{\mathcal{M}}$) mirror baryons. The third and fifth columns denote the collapse redshifts in the $\mathcal{O}$ and $\mathcal{M}$ sectors, respectively.

Model No	Halo mass$^{\mathcal{O}}$ $M_\odot$	Collapse redshift$^{\mathcal{O}}$ z	Halo mass$^{\mathcal{M}}$ $M_\odot$	Collapse redshift$^{\mathcal{M}}$ z
1	3.5×10^5	23.3	1.01×10^7	13.79
2	1.3×10^6	20	2.69×10^7	14.05
3	7.8×10^5	24.5	1.3×10^7	13.35
4	6.7×10^5	25.4	1.2×10^7	16

primordial species (H, H^+, H^-, He, He^+, He^{++}, H_2, H_2^+, e^-)[1] in cosmological simulations. Our chemical model includes the most important gas-phase reactions and processes including the formation of molecular hydrogen. It also includes the cooling and heating processes due to collisional excitation, collisional ionization, radiative recombination, collisional induced emission, H_2, and chemical heating/cooling.

Simulations of the $\mathcal{O}$ and $\mathcal{M}$ sector are performed with the same procedure. Because of the nature of the mirror sector, its chemistry is the same as for the ordinary baryons, see D18 for further details. The only difference is due to the initial conditions. For the $\mathcal{M}$ sector with $x = 0.01$, the $\mathcal{M}$ helium fraction is almost negligible (Berezhiani 2005). More importantly, the initial abundance of free $\mathcal{M}$ electrons at $z = 100$ is about four orders of magnitude smaller than the ordinary one (see fig. 1 of D18) and we scale the fractions of other species accordingly. We assume that the chemical properties (such as reaction rates, cooling and heating rates etc.) of mirror baryons are similar to the $\mathcal{O}$ sector as they are the mirror copy of the standard model, see D18 for further details.

3 RESULTS

We present the main findings of this work in this section. In total, we have performed eight cosmological simulations for four different haloes in both sectors. The properties of the simulated haloes are listed in Table 1. In the coming subsections, we discuss and compare the thermal and chemical evolution of the haloes in both sectors. We also point out the differences in the fragmentation properties of the haloes.

3.1 Time evolution of a reference run in the mirror and ordinary sector

We take halo 1 as the reference case and compare its thermal evolution in both sectors as shown in Fig. 1. The temperature of the gas in the $\mathcal{M}$ sector at $z = 100$ is lower than in the $\mathcal{O}$ sector due to inefficient Compton heating. As collapse proceeds gas falls into the DM potential and gets heated up to about 1000 K due to the virialization shocks. In the $\mathcal{O}$ sector, gas starts to cool and collapse after reaching the molecular hydrogen cooling threshold (a few times $10^5\,M_\odot$) at $z = 23$. In the $\mathcal{M}$ sector, due to the inefficient production of molecular hydrogen, gas cannot cool until the halo mass reaches the atomic cooling limit. Consequently, the halo virial temperature reaches around 10^4 K and the halo mass $\geq 10^7\,M_\odot$. For the $\mathcal{M}$ sector, strong shocks during the virialization of an atomic cooling halo catalyse H_2 formation by enhancing the electron fraction and as a result H_2 abundance gets significantly increased.

Once sufficient $\mathcal{M}$ H_2 has formed, the gas temperature is brought down to about a few hundred Kelvin in the core of the atomic cooling halo. Overall, the temperature in the centre of $\mathcal{M}$ haloes is about a factor of 2 higher compared to the $\mathcal{O}$ sector. The halo mass is about a factor of 20 larger and the collapse is delayed until $z \sim 14$, see Table 1. This suggests that the first haloes forming in the $\mathcal{M}$ sector are atomic cooling haloes while in the $\mathcal{O}$ sector minihaloes are formed first. This will have important implications for the early structure formation, see our discussion below.

3.2 Comparison of different haloes and fragmentation study

We here compare the chemical and thermal evolution of four different haloes in the $\mathcal{M}$ sector only. Unless noted otherwise, the quantities in the following description refer to the mirror sector. The plots of H_2 and H II mass fractions and temperature against the gas density at the collapse redshifts of the haloes are shown in Fig. 2. The H II fraction at low densities is about 10^{-7}, a few orders of magnitude lower compared to the $\mathcal{O}$ sector and reaches up to $\sim 10^{-4}$ at densities between 10^{-26}–10^{-24} g cm^{-3} due to the strong virialization shocks. At higher densities, the H II fraction starts to decline due to the Lyman alpha and molecular hydrogen cooling which brings the temperature down. This trend has been observed for all haloes. The enhanced electron fraction during the process of virialization acts as a catalyst for the formation of molecular hydrogen and as a result the H_2 fraction gets boosted about six orders of magnitude. After the halo has virialized, the H_2 fraction continues to increase and gets further enhanced due to the three body reactions. The typical abundance of H_2 in the core of the halo is a few times 10^{-2} and the same is for all haloes. Overall, the haloes with higher virial masses have higher H II and H_2 fractions.

Contrary to the $\mathcal{O}$ sector, the temperature of the halo continues to increase until it reaches the atomic cooling regime due to the low H_2 fraction at earlier times. By that time, the halo mass is above $10^7\,M_\odot$ and Lyman alpha cooling becomes effective at densities above 10^{-24} g cm^{-3}. After reaching the atomic cooling limit, the molecular hydrogen formed during virialization brings the gas temperature down to a few hundred Kelvin. Consequently, the formation of minihaloes remains suppressed in the $\mathcal{M}$ sector. To further clarify the differences between two sectors, we show the averaged radial profiles of H_2 and H II mass fractions for both sectors in Fig. 3. Although the initial abundances of H_2, H II, H I, and electrons are a few orders of magnitude lower in the $\mathcal{M}$ sector, they become almost similar to the $\mathcal{O}$ sector after virialization. Due to the larger halo mass in $\mathcal{M}$ sector, stronger virialization shocks boost the abundances of these species and reduce the differences between the two sectors.

[1]From now on, instead of using chemical notation for H^+ and H, we use H II and H I, respectively.

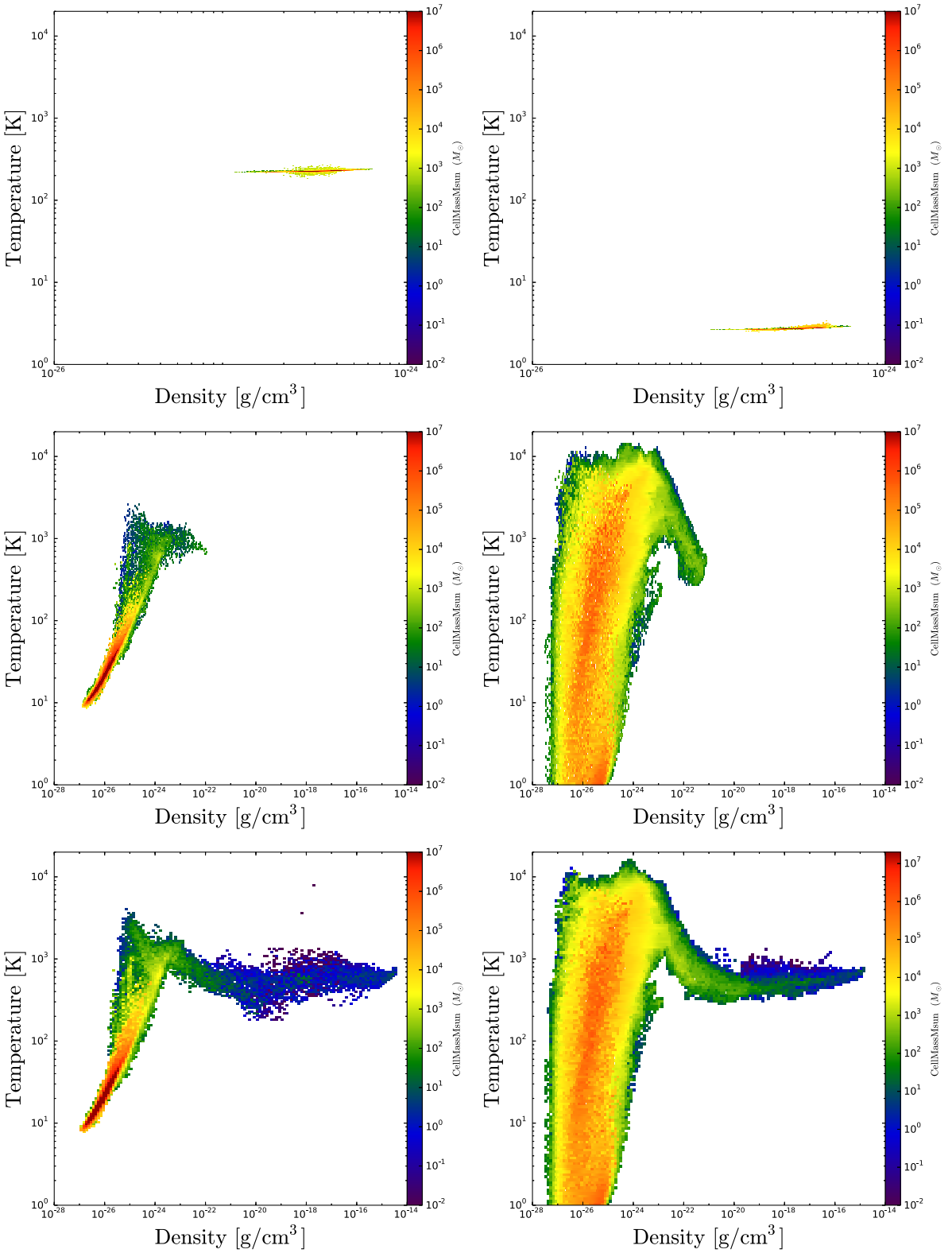

Figure 1. Phase plots of the temperature in the reference halo for both the $\mathcal{O}$ (left) and the $\mathcal{M}$ (right) sectors. The top row shows the initial redshift, the middle row the virialization redshift, and the bottom row the collapse redshift.

To compare the dynamical properties of the haloes in both sectors, we show the profiles of the temperature, density, enclosed mass, and the mass inflow rates in Fig. 4. The density in the outskirts of the halo is 10^{-24} g cm^{-3} and increases up to 10^{-16} g cm^{-3} in the core, with small bumps due to the presence of substructure. The density profiles are almost similar in both sectors for all haloes and follow

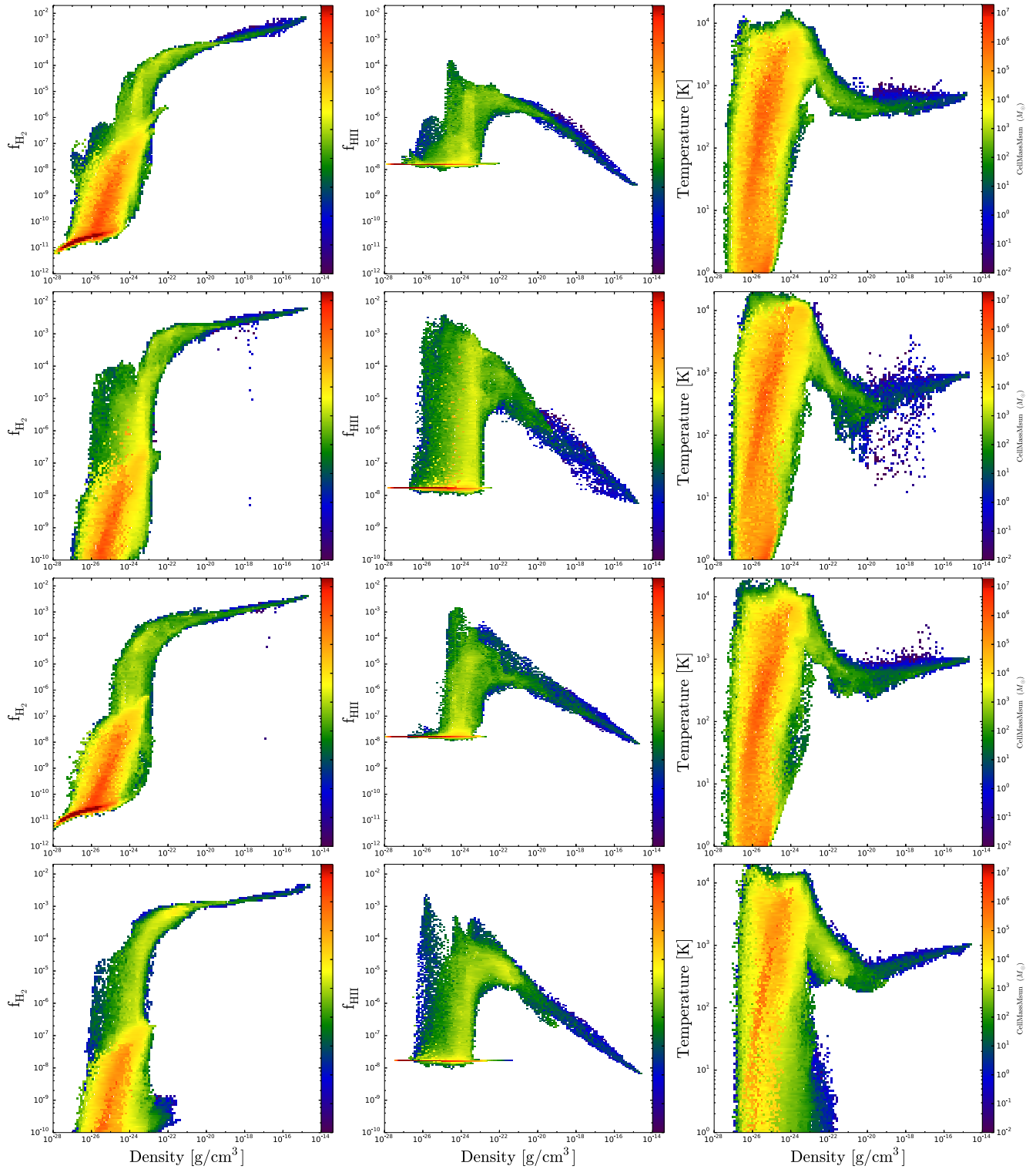

Figure 2. Phase plot of H_2 and H II mass fractions and temperature against gas density for four haloes in the mirror sector. Each row represents a different halo at its collapse redshift, as listed in Table 1.

the $\sim R^{-2.1}$ behaviour as expected for H_2 cooled gas. Consequently, the enclosed gas mass profiles are similar in both sectors, but almost an order of magnitude larger around 100 pc in the $\mathcal{M}$ sector. This difference comes from the larger halo masses in the $\mathcal{M}$ sector. The temperature profiles show that differences between the two sectors are very prominent above 10 pc. For instance, at 100 pc the temperature in the $\mathcal{M}$ sector is about 8000–10^4 K while in the $\mathcal{O}$ sector the temperature does not exceed 10^3 K. These differences are again due to the larger halo masses and virial temperatures in the $\mathcal{M}$ sector. In general, gas in the centre of the haloes is warmer in

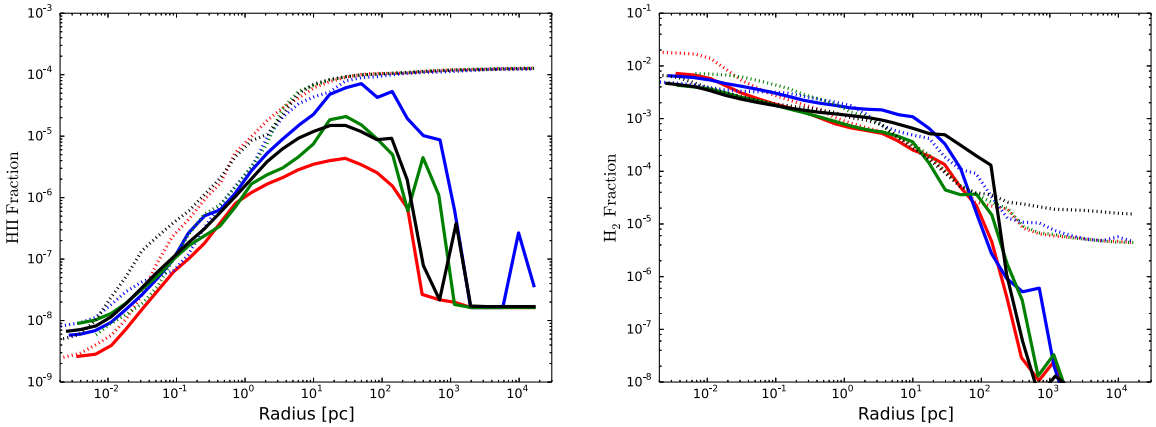

Figure 3. Spherically averaged and radially binned profiles of the H II and H_2 mass fractions. The solid lines represent haloes in the mirror sector while dashed lines are for the haloes in the ordinary sector, as listed in Table 1, all computed at the collapsed redshift. The colours red, blue, green, and black represent haloes 1, 2, 3, and 4, respectively.

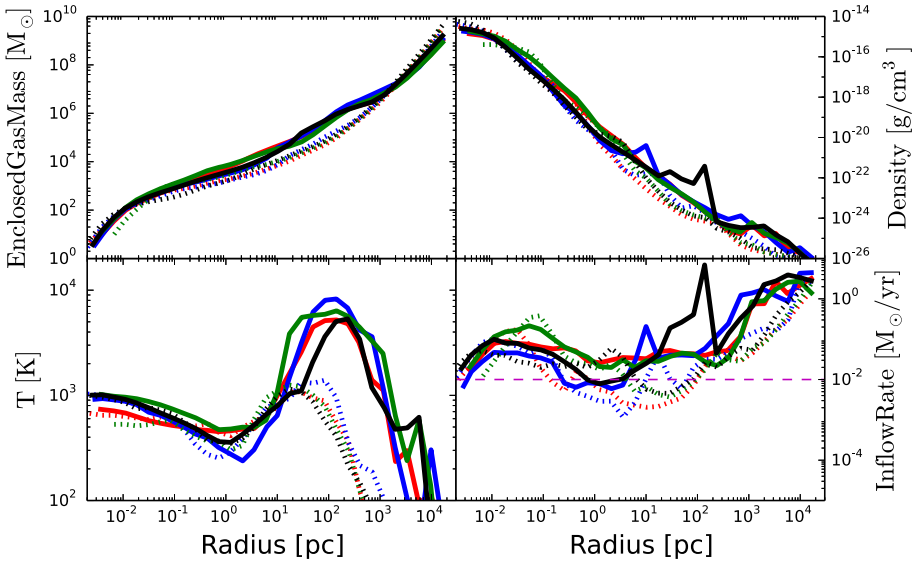

Figure 4. Spherically averaged and radially binned profiles of gas density, temperature, enclosed gas mass, and mass inflow rates. The solid lines represent haloes in the mirror sector while dashed lines are for the haloes in the ordinary sector, all computed at the collapsed redshift, as listed in Table 1. The colours red, blue, green, and black represent haloes 1, 2, 3, and 4, respectively.

the $\mathcal{M}$ sector. The average mass inflow rates for both sectors are between 0.001 and 0.1 $M_\odot$ yr^{-1} and they are generally lower in the $\mathcal{O}$ sector.

The morphology of the haloes at their collapse redshifts is shown in Fig. 5. The density structure in the central region of the halo is different for both sectors and this trend is observed for all haloes. In general, for the $\mathcal{O}$ sector the density structure is more dense, filamentary, and compact compared to the $\mathcal{M}$ one. Moreover, there is more than one gas clump, and they are well separated, while in the $\mathcal{M}$ sector structures are more spherical and fluffy. This comes from the fact that the molecular hydrogen is mainly concentrated in the core of the halo in the $\mathcal{M}$ sector while in the outskirts of the halo H_2 is below the universal value (i.e. 10^{-3}). Due to the lower temperatures and pressures, more fragmentation is expected in the $\mathcal{O}$ sector. However, the possibility of fragmentation at the later stages of collapse in the $\mathcal{M}$ sector cannot be completely ruled out.

4 DISCUSSION AND CONCLUSIONS

In this study, we have investigated the possibility of BH formation in the context of dissipative DM. Previous works (D18) suggest that a small component of DM similar to the **ordinary** baryonic matter may collapse to form massive BHs. D18 have shown, employing one-zone models, that the evolution in the $\mathcal{M}$ sector is very different from the $\mathcal{O}$ one. Motivated by the work of D18, we have performed 3D cosmological simulations for four different haloes to explore the impact of hydrodynamics and collapse dynamics on the thermal and chemical evolution as well as their implications for structure formation.

For our simulations of the $\mathcal{O}$ sector, we use the standard ΛCDM cosmology. In the other set of simulations, we add the $\mathcal{M}$ sector. However, because of numerical difficulties, we neglect the ordinary baryons in the simulations with the $\mathcal{M}$ sector, thus effectively having only collisionless DM and mirror component. In fact, the potential influence of the ordinary baryons on the mirror ones is

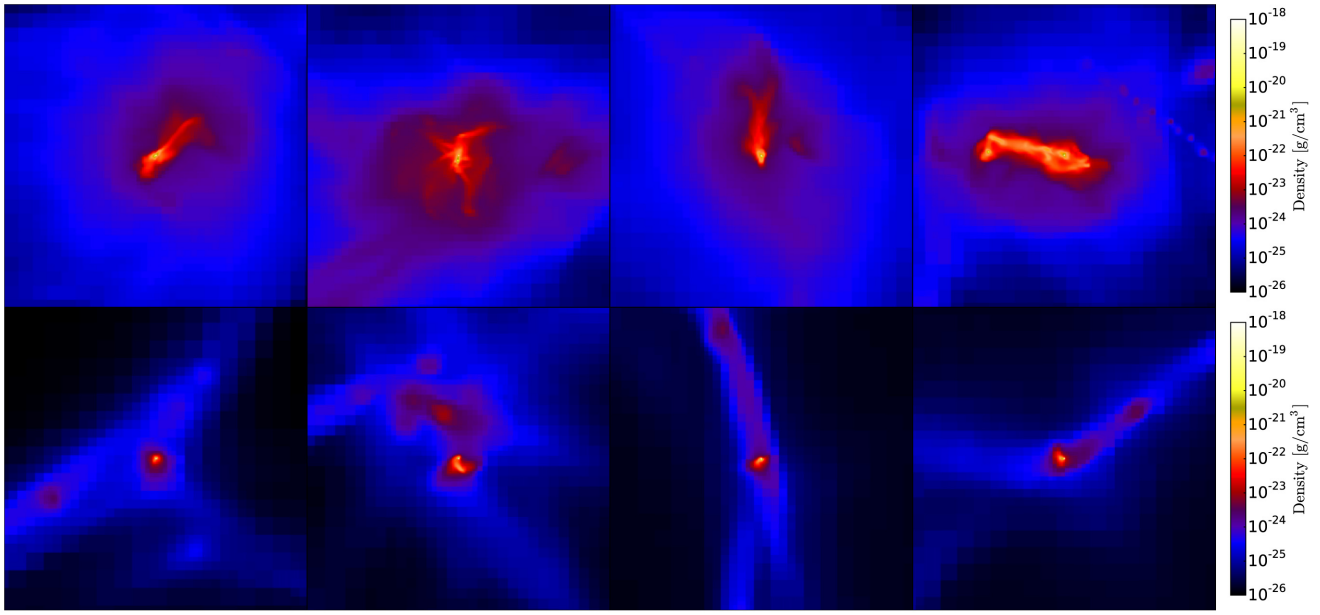

Figure 5. Density projections (the average density along the line of the sight) at the collapse redshifts of the haloes for the central 500 pc region. The top row shows haloes in the mirror sector while the bottom row corresponds to the ordinary sector.

only via gravity. Hence we expect that, due to inefficient cooling, the cloud will not be able to collapse even if we take into account the additional gravitational effect of baryons.

In general our results are in an agreement with the findings of D18. We show that the formation of minihaloes remains suppressed in the $\mathcal{M}$ sector due to the deficiency of molecular hydrogen and the gravitational collapse is significantly delayed by $\Delta z \sim 10$. Consequently, **mirror** gas keeps collapsing until the halo mass reaches an atomic cooling limit with typical halo masses of $10^7\,M_\odot$ and virial temperatures around 10^4 K. In the $\mathcal{M}$ sector, the abundances of H_2 and H II are a few orders of magnitude lower before the virialization of the haloes but become comparable to the respective abundances in the $\mathcal{O}$ sector after virialization because of strong shocks. In general, the H_2 mass fraction is about a factor of 2 lower and the temperature is about a factor of 2 higher. The mass inflow rate is $\geq 10^{-2}\,M_\odot\,yr^{-1}$, a factor of a few higher than in the baryonic sector. The haloes are also more spherical and fluffy, with one central mirror gas clump as opposed to several smaller gas clumps in the ordinary sector. The degree of fragmentation is expected to be much lower in the mirror sector.

Overall, haloes in the $\mathcal{M}$ sector are similar to haloes irradiated by a moderate background UV flux in the standard scenario (Schleicher, Spaans & Glover 2010; Latif et al. 2016b), but there are a few important differences. At earlier cosmic times (about $z \geq 15$), $\mathcal{M}$ haloes are expected to be more abundant and statistically different from haloes in the $\mathcal{O}$ sector irradiated by a moderate background UV flux. In the mirror component, we only modify the initial conditions, not the chemistry; on the contrary, in the background UV flux scenario, the production of H_2 is actively suppressed dynamically. This conclusion will of course be different in models where the hidden sector has a different chemistry than the ordinary baryons. In summary, we expect that the BH seeds formed in the $\mathcal{M}$ sector will have a larger abundance and smaller masses with respect to those obtained in the background UV models. Furthermore, when BHs form in the hidden sector the accretion rate is largely boosted because they can accrete a substantial portion of dissipative mirror DM. We expect that statistical investigations of collapsed objects at early times, particularly with 21 cm observations using SKA, could distinguish both scenarios depending on the number density of intermediate-mass BHs near $z \sim 20$.

All these factors suggest that the conditions for the formation of massive objects, including BHs, are more favourable in the $\mathcal{M}$ sector. Our results reinforce the findings of D18 and provide a viable alternative of massive BH formation at high redshift.

ACKNOWLEDGEMENTS

ML thanks the UAEU for funding via startup grant No. 31S372. AL acknowledges support from the European Research Council project No. 740120 'INTERSTELLAR'. DRGS thanks for funding via Conicyt PIA ACT172033, Fondecyt regular (project code 1161247), the 'Concurso Proyectos Internacionales de Investigación, Convocatoria 2015' (project code PII20150171) and the BASAL Centro de Astrofísica y Tecnologías Afines (CATA) PFB-06/2007. GDA is supported by the Simons Foundation Origins of the Universe program (Modern Inflationary Cosmology collaboration). This work has made use of the Horizon Cluster, hosted by Institut d'Astrophysique de Paris, to carry out and analyse the presented simulations. SB is financially supported by Fondecyt Iniciacion (project code 11170268), CONICYT programa de Astronomia Fondo Quimal 2017 QUIMAL170001, and BASAL Centro de Astrofisica y Tecnologias Afines (CATA) AFB-17002.

REFERENCES

Alvarez M. A., Wise J. H., Abel T., 2009, ApJ, 701, L133
Bañados E. et al., 2018, Nature, 553, 473
Barbieri R., Hall L. J., Harigaya K., 2016, J. High Energy Phys., 11, 172
Becerra F., Marinacci F., Bromm V., Hernquist L. E., 2018, MNRAS, 480, 5029

Berezhiani Z., 2005, Through the Looking-Glass Alice's Adventures in Mirror World. World Scientific Publishing Co, p. 2147
Berezhiani Z. G., Dolgov A. D., Mohapatra R. N., 1996, Phys. Lett., B375, 26
Berezhiani Z., Comelli D., Villante F. L., 2001, Phys. Lett., B503, 362
Blinnikov S. I., Khlopov M., 1983, Sov. Astron., 27, 371
Boekholt T. C. N., Schleicher D. R. G., Fellhauer M., Klessen R. S., Reinoso B., Stutz A. M., Haemmerlé L., 2018, MNRAS, 476, 366
Bromm V., Loeb A., 2003, ApJ, 596, 34
Bryan G. L. et al., 2014, ApJS, 211, 19
Chon S., Latif M. A., 2017, MNRAS, 467, 4293
D'Amico G., Panci P., Lupi A., Bovino S., Silk J., 2018, MNRAS, 473, 328(D18)
Davies M. B., Miller M. C., Bellovary J. M., 2011, ApJ, 740, L42
Dayal P., Rossi E.-M., Shiralilou B., Piana O., Choudhury T.-R., Volonteri M., 2018, preprint(arXiv:1810.11033)
Devecchi B., Volonteri M., Rossi E. M., Colpi M., Portegies Zwart S., 2012, MNRAS, 421, 1465
Essig R., McDermott S.-D., Yu H.-B., Zhong Y.-M., 2018, preprint(arXiv: 1809.01144)
Fan X. et al., 2003, AJ, 125, 1649
Foot R., 2004, Int. J. Mod. Phys., D13, 2161
Foot R., Vagnozzi S., 2015, Phys. Rev. D, 91, 023512
Grassi T., Bovino S., Schleicher D. R. G., Prieto J., Seifried D., Simoncini E., Gianturco F. A., 2014, MNRAS, 439, 2386
Hahn O., Abel T., 2011, MNRAS, 415, 2101
Haiman Z., 2013, in Wiklind T., Mobasher B., Bromm V., eds, Astrophysics and Space Science Library, Vol. 396, The First Galaxies. Springer-Verlag, Berlin, p. 293
Inayoshi K., Haiman Z., Ostriker J. P., 2016, MNRAS, 459, 3738
Jiang L. et al., 2009, AJ, 138, 305
Johnson J. L., Bromm V., 2007, MNRAS, 374, 1557
Katz H., Sijacki D., Haehnelt M. G., 2015, MNRAS, 451, 2352
Khlopov M. Yu., Beskin G. M., Bochkarev N. E., Pustylnik L. A., Pustylnik S. A., 1991, Sov. Astron., 35, 21
Kormendy J., Ho L. C., 2013, ARA&A, 51, 511
Latif M. A., Schleicher D. R. G., 2015, A&A, 578, A118
Latif M. A., Ferrara A., 2016a, Publ. Astron. Soc. Aust., 33, e051
Latif M. A., Omukai K., Habouzit M., Schleicher D. R. G., Volonteri M., 2016b, ApJ, 823, 40
Latif M. A., Schleicher D. R. G., Hartwig T., 2016c, MNRAS, 458, 233
Latif M. A., Volonteri M., Wise J. H., 2018, MNRAS, 476, 5016
Lupi A., Colpi M., Devecchi B., Galanti G., Volonteri M., 2014, MNRAS, 442, 3616
Lupi A., Haardt F., Dotti M., Fiacconi D., Mayer L., Madau P., 2016, MNRAS, 456, 2993
Madau P., Haardt F., Dotti M., 2014, ApJ, 784, L38
Mayer L., Fiacconi D., Bonoli S., Quinn T., Roškar R., Shen S., Wadsley J., 2015, ApJ, 810, 51
Mortlock D. J. et al., 2011, Nature, 474, 616
Planck Collaboration XIII, 2016, A&A, 594, A13
Portegies Zwart S. F., McMillan S. L. W., 2002, ApJ, 576, 899
Regan J. A., Downes T. P., Volonteri M., Beckmann R., Lupi A., Trebitsch M., Dubois Y., 2018, preprint (arXiv:1811.04953)
Reinoso B., Fellhauer M., Véjar R., 2018a, MNRAS, 476, 1869
Reinoso B., Schleicher D. R. G., Fellhauer M., Klessen R. S., Boekholt T. C. N., 2018b, A&A, 614, A14
Rosenberg E., Fan J., 2017, Phys. Rev. D, 96, 123001
Sakurai Y., Yoshida N., Fujii M. S., 2019, MNRAS, 484, 4665
Schleicher D. R. G., 2018, preprint (arXiv:1807.06055)
Schleicher D. R. G., Spaans M., Glover S. C. O., 2010, ApJ, 712, L69
Schleicher D. R. G., Palla F., Ferrara A., Galli D., Latif M., 2013, A&A, 558, A59
Smith B. D., Regan J. A., Downes T. P., Norman M. L., O'Shea B. W., Wise J. H., 2018, MNRAS, 480, 3762
Venemans B. P. et al., 2015, MNRAS, 453, 2259
Volonteri M., Bellovary J., 2012, Rep. Prog. Phys., 75, 124901
Wise J. H., Regan J.-A., O'Shea B. W., Norman M. L., Downes T.-P., Xu H., 2019, Nature, 566, 85,
Willott C. J. et al., 2007, AJ, 134, 2435
Woods T. E. et al., 2018, preprint (arXiv:1810.12310)
Wu X.-B. et al., 2015, Nature, 518, 512

This paper has been typeset from a TEX/LATEX file prepared by the author.